Catalysis Science & Technology

ROYAL SOCIETY OF CHEMISTRY

PAPER

View Article Online
View Journal | View Issue

Cite this: *Catal. Sci. Technol.*, 2024, **14**, 4198

Elucidating the role of the state of Pd in the H_2-SCR of NO_x by operando XANES and DRIFTS†

Thomas J. Eldridge, *[ab] Michael Borchers,[b] Patrick Lott, [b] Jan-Dierk Grunwaldt [ab] and Dmitry E. Doronkin *[ab]

The selective catalytic reduction (SCR) of NO_x with hydrogen is an attractive strategy for NO_x removal when H_2 is used as a sustainable fuel in combustion engines. However, the pathway suffers from a strong overconsumption of H_2 *via* direct oxidation to water. In order to improve the understanding of the SCR mechanism with H_2 as the reductant, the state of the active metal, the reactive surface intermediates, and the conditions which are suited for efficient SCR need to be uncovered. A 1%Pd/5%V_2O_5/20%TiO_2–Al_2O_3 catalyst was investigated using *operando* X-ray absorption spectroscopy (XAS) and diffuse reflectance infrared Fourier-transform spectroscopy (DRIFTS) to track the temperature dependent structure and state of Pd, as well as its gradients and surface intermediates. XAS shows that NO reduces oxidized Pd, forming metal-support interfacial nitrates according to DRIFTS. Partially reduced Pd becomes oxidized by reducing interfacial NO_x species to Pd-nitrosyls. Limitations for the H_2-SCR of NO_x arise from the balance of adsorbed Pd–NO and activated H_2, which is dependent on Pd state. The bulk metallic Pd which forms above 250 °C causes a runaway activation of H_2, further reduction of Pd, and loss of nitrosyls on Pd. The highest activity occurs when Pd is oxidized enough to promote metal-support interfacial nitrates and also reduced enough to convert these nitrates to Pd-nitrosyls. The storage of NO_x and formation of NH_x on vanadia–titania permits conversion of NO at high temperatures, but does not counteract the deactivation of Pd. In conclusion, activation of H_2 is favored on metallic sites, but must be moderated to allow for PdO being present as well.

Received 2nd May 2024,
Accepted 25th June 2024

DOI: 10.1039/d4cy00574k

rsc.li/catalysis

Introduction

In the course towards reducing carbon-based engine-out emissions and because of its potential future production from sustainable sources,[1,2] hydrogen has been investigated as an attractive alternative to diesel in thermal combustion engines. Apart from being a potential sustainable energy carrier, the primary motivation for using H_2 is the avoidance of carbon and particulate matter (PM) emissions in the exhaust. However, under the high temperatures of H_2 combustion, N_2 oxidation by O_2 from air leads to NO_x as a pollutant in the 1000 ppm range. While these NO_x emissions can be mitigated by optimal air-to-fuel ratios and engine control methods,[3–5] H_2 thermal combustion engines have a higher NO_x emission potential relative to traditional fuels.[6]

In order to meet NO_x emission guidelines, an emission-out catalyst for the selective catalytic reduction (SCR) of NO_x is necessary. At present, SCR of NO_x is largely executed using NH_3 as the reductant.[7–13] However, due to the direct availability from the fuel tank, H_2 has been investigated as an alternative SCR agent.

Current catalysts for SCR of NO_x by H_2 show higher levels of NO_x conversion, relative to NH_3 as the reducing agent, at lower temperatures.[14,15] However, the primary challenge of H_2-SCR is combatting the competitive direct oxidation of H_2 to H_2O, which becomes the favored reaction pathway at high temperatures. Further complications include several reactions simultaneously occurring over the catalyst bed, including NH_3 formation and subsequent NH_3-SCR, leading to gradients in reaction product concentrations and in catalyst structure.[16,17]

Supported noble metal catalysts, with favor towards Pt[18–23] and Pd,[24–29] are most widely investigated for H_2-SCR. Pt and Pd present different benefits and challenges relative to other noble metals: where Pt shows substantially higher NO_x conversion but lower selectivity for N_2 with respect to N_2O, and where Pd has high selectivity for N_2 but lower overall catalytic activity.[15]

[a] *Institute of Catalysis Research and Technology, Karlsruhe Institute of Technology, Eggenstein-Leopoldshafen 76344, Germany. E-mail: thomas.eldridge@kit.edu, dmitry.doronkin@kit.edu*
[b] *Institute for Chemical Technology and Polymer Chemistry, Karlsruhe Institute of Technology, Karlsruhe 76131, Germany*

† Electronic supplementary information (ESI) available. See DOI: https://doi.org/10.1039/d4cy00574k

There are several primary groups of catalyst supports that have been studied in H_2-SCR: (1) TiO_2,[28–32] often combined with V_2O_5,[26,27,33,34] (2) WO_3/ZrO_2,[35–38] and (3) MgO–CeO_2,[19–21] and (4) zeolites, alone or in combination with other supports.[39–43] H_2-SCR catalysts with low noble metal loadings (<1 wt%) of Pt or Pd on WO_3/ZrO_2 or MgO-CeO_2 have shown wide temperature ranges (100 to 400 °C) of NO_x conversion with high (>80%) selectivity for N_2. However, they have not been studied as extensively as catalysts supported on TiO_2. Pd on TiO_2–Al_2O_3 is notable for converting NO_x over a wide temperatures range from 100 to 350 °C, but with a significant drop in activity at 200 °C.[26,30] This phenomenon was explained by NO reduction to N_2, occurring from 100 to 200 °C, NO oxidation to NO_2, occurring from 200 to 400 °C, and NO_2 reduction to N_2 at 100 to 400 °C. The addition of V_2O_5 to Pd/TiO_2–Al_2O_3 followed a study with Pd/V_2O_5/Al_2O_3 which showed high levels of NO reduction to N_2 in the narrow range of 200 to 300 °C,[33] which well counteracted the observed activity decrease on Pd/TiO_2–Al_2O_3.[26]

In order to better understand the reactive conditions of Pd/V_2O_5/TiO_2–Al_2O_3 for H_2-SCR of NO_x, a study was performed using a honeycomb monolith and a variety of concentrations of NO, H_2, and O_2.[34] It was shown that the H_2 reaction pathway plays a significant role, where NO reduction to N_2 occurred more readily when either H_2 amounts were increased or O_2 concentration decreased, as O_2 competes with NO for reaction with H_2. Additionally, the catalyst state (*e.g.* Pd oxidized/reduced, Pd particles or clusters) was shown to play a significant role in SCR activity, as the pre-reduced catalyst showed significantly higher activity and N_2 selectivity at temperatures below 200 °C.

In order to gain further insight into the surface reactions and the mechanism, *ex situ* characterization and catalytic activity studies, which use outlet gas beyond the catalyst, are not sufficient for observing what occurs within the black-box catalyst. For this purpose, *operando* and *in situ* characterization is need to unravel the species and structure of the catalyst as a function of time and space while the reaction is ongoing.[44] Spectroscopic techniques, such as X-ray absorption spectroscopy (XAS) and diffuse reflectance infrared Fourier-transformed spectroscopy (DRIFTS) are able to measure the bulk and surface state of catalysts during steady-state and transient chemical reactions. These techniques also enable the measurement of spatial gradients in surface species concentration and catalyst state[45–47] and are thus applied during H_2-SCR in this study. Herewith, the present work aims at linking the oxidation state of Pd to the catalytic hydrogen combustion and selective catalytic reduction of NO_x by H_2 under dynamic reaction conditions. Both *operando* spatially and time-resolved XAS and *operando* DRIFTS measurements were conducted on a 1%Pd/V_2O_5/TiO_2–Al_2O_3 catalyst.

Experimental

A 1%Pd/5%V_2O_5/20%TiO_2–Al_2O_3 catalyst was prepared *via* the following steps: γ-Al_2O_3 (Puralox, Sasol) was calcined in air for 5 h at 700 °C and suspended in a solution of $Ti(OBu)_4$ (Merck) and EtOH (≥99.8%, VWR Chemicals); $Ti(OBu)_4$ was hydrolyzed by dropwise addition of deionized water to the suspension and rigorous stirring. The received TiO_2–Al_2O_3 solid was dried for 2 h at 70 °C and calcined in air for 6 h at 500 °C. V_2O_5 was added to the 20 wt.% TiO_2–Al_2O_3 support *via* incipient wetness impregnation (IWI) using a NH_4VO_3 (Alfa Aesar) solution with aqueous oxalic acid (Merck) and subsequent drying for 1 h at 70 °C and calcination in air for 12 h at 500 °C. Pd was added in a second IWI using an aqueous $Pd(NH_3)_4(NO_3)_2$-solution (abcr) and calcination of the received catalyst powder for 16 h at 500 °C. Inductively coupled plasma optical emission spectroscopy (ICP-OES) confirmed the target elemental composition of the catalyst.

N_2-physisorption of the catalyst powder was measured using a BELSORP-mini II instrument (BEL Japan) with pretreatment under vacuum at 300 °C for 2 h. Analysis of the adsorption–desorption curve by the Brunauer–Emmett–Teller (BET) method yielded the specific surface area and total pore volume of the catalyst.

X-ray diffraction (XRD) patterns were acquired with an X'PERT PRO diffractometer (PANalytical) using a Cu-Kα radiation source with a wavelength of 1.54 Å (2θ from 20 to 80°, step size of 0.017°, acquisition time of 0.44 s per data point).

Temperature-programmed reduction by hydrogen (H_2-TPR) was performed from 40 to 600 °C at 10 K min^{-1} in a 50 mL min^{-1} flow of 10% H_2 in Ar using an AutoChem II Chemisorption Analyzer (Micromeritics). A thermal conductivity detector (TCD) measured H_2 consumption. Prior to H_2-TPR, the sample was pretreated by heating with a temperature ramp of 10 K min^{-1} up to 500 °C under 20% O_2 in N_2.

Operando X-ray absorption spectroscopy (XAS) measurements were obtained at the PETRA III P64 beamline[48] at DESY (Hamburg, Germany). Catalyst powder was pressed and sieved to 125–250 μm grains to minimize mass transport limitations. The sieved fraction was placed between two quartz wool plugs in a fixed-bed quartz capillary serving as plug-flow microreactor.[49] The microreactor was heated by a hot air gas blower (Leister LE mini kit). Using capillary microreactors of 2 mm outer diameter and 0.02 mm wall thickness loaded with 12.5 mg of the granulated catalyst for a bed length of 4.1 mm, NO conversion was measured by a mass spectrometer (MS, Hiden ExQ) at the outlet, while simultaneously recording time-resolved X-ray absorption near edge structure (XANES) spectra at different positions along the catalyst bed, under a 50 mL min^{-1} flow (GHSV 60 000 h^{-1}) of 1000 ppm NO, 5000 ppm H_2, and 10% O_2 (He balance) in different gas combinations, following the sequential order as shown in Table 1; between each gas mixture, the setup pipes and the reactor itself were flushed with He. The sample was oxidized in 10% O_2 at 500 °C prior to TPR. A single light-off-light-out cycle from 25 to 350 °C at 2 K min^{-1} was performed for each gas mixture during continuous XANES measurements.

Due to time limitations at the XAS beamline, only two-point calibrations (zero gas and educts at zero conversion) of MS instrumentation were possible and allowed for only

Table 1 Volumetric inlet gas compositions for the XANES/DRIFTS catalytic activity measurements (He/Ar balance), provided in the order (top-to-bottom) introduced to the $Pd/V_2O_5/TiO_2–Al_2O_3$ catalyst

Gas mix	NO (ppm)	H_2 (ppm)	O_2 (%)
TPO	0	0	10
NOA	1000	0	10
SCR	1000	5000	10
MixA	0	5000	10
NOB	1000	0	0
MixB	1000	5000	0
TPR	0	5000	0

qualitative and semi-quantitative analysis. Additionally, small quantities (*i.e.* <100 ppm) of nitrogen species such as NH_3, N_2, N_2O, and NO_2 measured at m/z values of 15, 28, 44, and 46 were particularly difficult to detect by MS and did not produce enough counts for robust quantitative analysis.

Quick extended X-ray absorption fine structure (QEXAFS) spectra[50] were obtained with a monochromator frequency of 1 Hz, resulting in 2 spectra per second. The polychromatic X-ray beam from the tapered undulator was tuned to the Pd K edge by a liquid nitrogen cooled Si(111) channel-cut crystal monochromator. With a beam size of 1.0 mm (horizontal) × 1.0 mm (vertical), 4 points along the catalyst bed were measured. For the spatially resolved XANES evaluation, the positions were continuously cycled during light-off and the constantly running QEXAFS measurements, holding at each position for 30 seconds; timestamps were recorded before and after each movement of the reactor to isolate and average spectra obtained at each position in order to improve the signal quality. Pd foil measured simultaneously with the catalyst served as the reference.

For evaluation of the XANES spectra, the QEXAFS data were read-in, split, and exported as text files using the JAQ Analyzes QEXAFS software (version 5.3).[48] Using a Python (version 3.10) script empowered by the Larch (version 0.9.65) package,[51] XANES spectra were calibrated for energy, sorted and averaged by position, and correlated with light-off temperature values. Normalization of spectra and subsequent linear combination analysis (LCA) were performed using the Athena software from the Demeter software package (version 0.9.26),[52] across an energy range from 24 340 to 24 400 eV, using the as-prepared $Pd/V_2O_5/TiO_2–Al_2O_3$ catalyst in oxygen and H_2 after temperature-programmed oxidation and reduction at 350 °C, respectively, as references.

DRIFTS spectra were obtained using a Vertex 70 spectrometer (Bruker) equipped with a Praying Mantis mirror assembly (Harrick) and a liquid nitrogen cooled mercury cadmium telluride (MCT) detector with a resolution of 4 cm^{-1}. A Praying Mantis high temperature reaction chamber (Harrick) with flat CaF_2 windows was loaded with 24.5 mg granulated catalyst (125–250 μm). Steady-state DRIFTS spectra were recorded as an average of 300 scans at 40 kHz at 25 °C intervals from 50 to 325 °C, approximating a single light-off-light-out cycle, with a flow of 50 ml min^{-1} (GHSV 30 000 h^{-1}) using the same pretreatment, gas mixtures, and sequence as with the XAS measurements and as described in Table 1, but using argon instead of helium for balance. Background reference interferograms were collected at each temperature once during cooling down after the initial oxidation pretreatment (10% O_2, 325 °C, 30 min). For DRIFTS quantitative analysis and comparison, the baseline of the pseudo-absorbance spectra was zeroed and flattened using a piecewise cubic Hermite interpolating polynomial (PCHIP) function.

Results and discussion

Characterization and catalytic activity of $Pd/V_2O_5/TiO_2–Al_2O_3$

The characterization data, light-off conversion profiles, product selectivity, and reaction pathway selectivity for this catalyst have previously been reported in great detail on the same catalyst coated on a honeycomb.[34] Hence, the results reported herein are discussed with respect to the outlet mass spectrometer measurements for the purpose of relating data from the XAS and DRIFTS measurements to the activity profile in the specific *operando* measurements. Fig. 1a and b show the light-off curves for NO reduction in the presence of H_2 and the H_2-SCR of NO, respectively.

The atypical light-off observed in Fig. 1a is due to the absence of O_2, matching well with the honeycomb study which showed that the NO conversion curve broadens and shifts to lower temperatures when the ratio of O_2 to H_2 is lowered. Over-stoichiometric conversion of H_2 and the gradual increase in H_2O MS intensity in the absence of NO during NO reduction by H_2, as shown in Fig. 1a, is due to the broad reduction area from 200 to 600 °C previously shown[34] by H_2-TPR for this catalyst. The change in the MS zero line for N_2O suggests conversion of trace N_2O impurities present in the NO gas cylinder available at the synchrotron.

Due to inherent differences between testing monolith and powder catalysts, under identical SCR gas conditions, the powder catalyst of this study underwent light-off for NO and H_2 conversion at higher temperatures relative to the monolith catalyst (*cf.* Fig. 1b); however, it is possible to correlate changes in the Pd state and surface species with the light-off and relate these data to the previously reported honeycomb catalyst study. This will be discussed in more detail below in combination with DRIFTS and XAS analysis below.

With exception to N_2O in Fig. 1a, nitrogen species products formed in amounts below the detection limit of the MS instrumentation; however, product selectivity under these gas conditions has been previously reported[34] and is out of the scope of this study. MS data measured during other gas conditions are shown in Fig. S1.† The relatively low O_2 conversion in Fig. 1b is due to the stoichiometric excess of O_2 used; Fig. S2† shows the absolute concentrations of H_2, NO, and O_2. From these data, a slight delay between the onset of SCR activity at 200 °C and increased O_2 conversion at 230 °C was observed, at which point the conversion of NO stagnated. This matches well with previous findings with the honeycomb catalyst where it was concluded that the direct oxidation of H_2 predominantly opposes H_2-SCR activity at elevated temperatures.

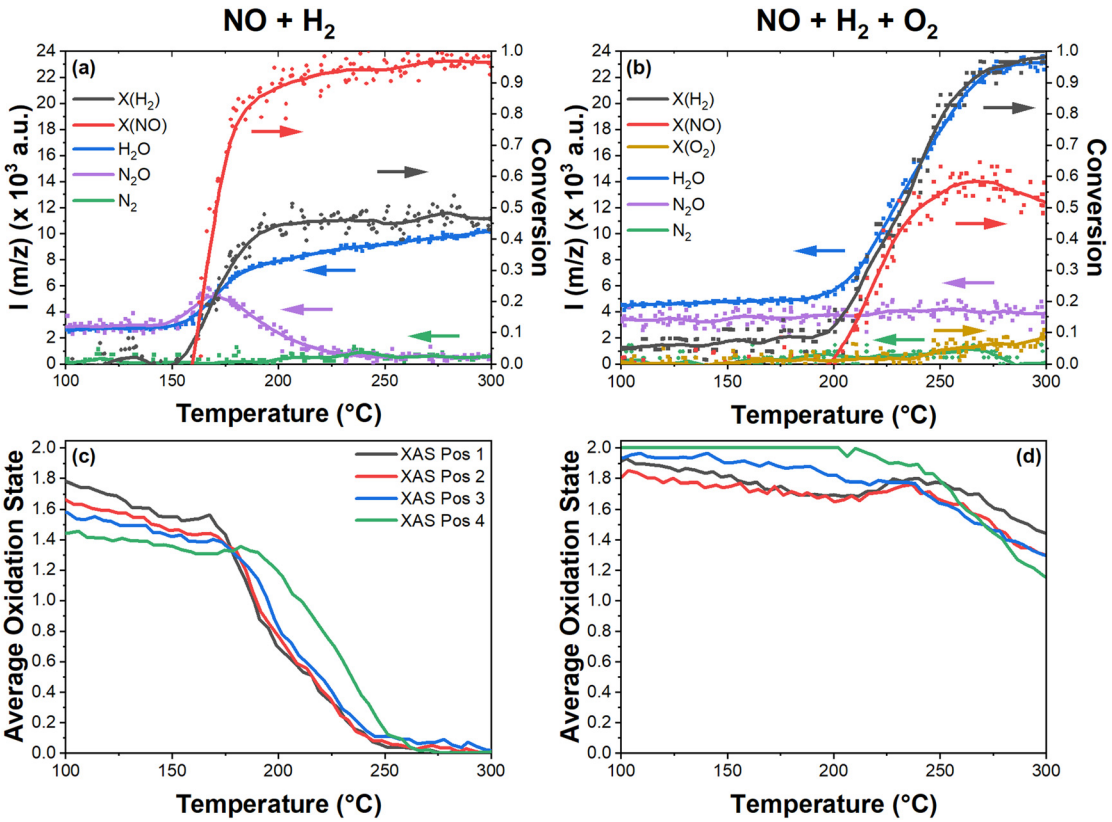

Fig. 1 Light off curves on 1%Pd/5%V_2O_5/20%TiO_2–Al_2O_3 (heating ramp of 2 K min^{-1}, 50 mL min^{-1}/GHSV 60 000 h^{-1}) during conversion of H_2, NO, and O_2 to H_2O, N_2, and N_2O (MS intensities at m/z = 2, 30, and 32 and 18, 28, and 44, respectively) in (a) 1000 ppm NO, 5000 ppm H_2 in He and (b) 1000 ppm NO, 5000 ppm H_2, and 10% O_2 in He (SCR); the dots are experimental data and the solid lines are locally weighted scatterplot smoothing (LOWESS) regressions; (c and d).

Operando XANES measurements

In order to elucidate the dynamic changes in the Pd oxidation state during H_2-SCR over the 1%Pd/5%V_2O_5/20%TiO_2-Al_2O_3 catalyst, QEXAFS measurements were performed with different gas mixtures. The resulting XANES spectra were quantified by LCA using corresponding reference spectra. Reference spectra for metallic/reduced Pd and oxidized Pd were obtained from 5000 ppm H_2 in argon (TPR) and 10% O_2 in argon (TPO) measurements, as shown in the ESI† by Fig. S3; LCA fits for these spectra were done using Pd foil and PdO references to confirm the catalyst had fully reduced and oxidized during TPR and TPO, respectively. Further analysis of the extended X-ray absorption fine

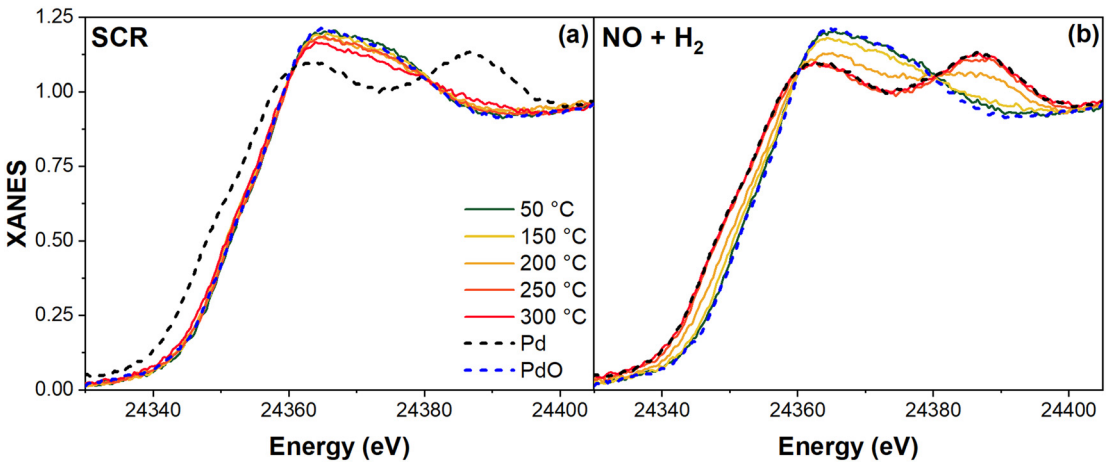

Fig. 2 Temperature dependent XANES spectra at the Pd K-edge for the 1%Pd/5%V_2O_5/20%TiO_2-Al_2O_3 catalyst during the (a) 1000 ppm NO, 5000 ppm H_2, and 10% O_2 in Ar (H_2-SCR) and (b) 1000 ppm NO and 5000 ppm H_2 in Ar.

structure (EXAFS) of the fully reduced Pd yielded an average Pd coordination number of 8.1 (*cf.* Table S1†), corresponding to nanoparticles of approximately 1 nm in diameter assuming a fcc full truncated cubooctahedral particle.[53]

Sample XANES spectra for the H_2-SCR (1000 ppm NO, 5000 ppm H_2, and 10% O_2 in argon) and NO reduction (1000 ppm NO and 5000 ppm H_2 in argon) gas conditions along with metallic Pd and PdO reference spectra are shown in Fig. 2. The LCA fits to these spectra are shown in Fig. 1c and d for the SCR and NO reduction conditions, respectively, showing space-resolved dynamic changes in the average oxidation state of Pd.

In the SCR reaction mixture, Pd is mostly in the oxidized state (Fig. 1d), gradually reducing with increasing temperature from 50 to 200 °C, with the beginning of the catalyst bed more reduced than the end. At the onset of SCR activity at 200 °C, the catalyst front oxidizes slightly, matching the conversion curve of NO shown in Fig. 1b. A local maxima of oxidation was reached at 250 °C, correlating with the maximum NO conversion. The subsequent Pd reduction matches the decrease in NO conversion from 250 to 300 °C. Spatially, the front of the catalyst bed reduces more from 50 to 200 °C and the end is generally more oxidized before the onset of SCR activity at 200 °C. From 200 to 300 °C, an inversion occurs such that the end of the catalyst bed is more reduced than the front. In the absence of DRIFTS data, the increase in Pd oxidation state during NO conversion suggests that Pd assists H_2 in the reduction of adsorbed NO species leading to the formation of N_2O or N_2. When considering the competing oxidation and reduction of Pd by O_2 and H_2, respectively, the alternate explanation for the oxidation of Pd from 200 to 250 °C is the loss of H_2 due to conversion during the H_2-SCR reaction. However, this is not likely to be the case. The substantial reduction of Pd above 250 °C, which was not observed with the NO + O_2 and H_2 + O_2 gas conditions (*cf.* Fig. S3†), indicates that H_2 and NH_x continue to reduce Pd even when participating in separate reactions. While the oxidation of Pd by O_2 is sufficient to counteract PdO reduction by H_2, reduced NH_x species limit the reoxidation of Pd by O_2. The role of NO in the oxidation of Pd will be discussed in further detail in the DRIFTS analysis below.

For the NO reduction condition (without O_2), at lower temperatures (50 to 150 °C) Pd is slightly reduced yet mostly oxidized with an average oxidation state of ~1.6 (Fig. 1c), with the end of the catalyst more reduced than the front. Pd gradually reduces in the presence of NO and H_2 until 168 °C where all positions rapidly reduce to Pd^0, with a temperature-dependent delay (ΔT) of 5 and 32 °C towards the end of the catalyst bed at positions 3 and 4, respectively. The onset of NO conversion occurs at 150 °C (before the rapid reduction in Pd, *cf.* MS data shown in Fig. 1a). Instead of correlating directly with NO reduction, the Pd oxidation state profile matches the diminishing production of N_2O. This suggests that H_2 partially reduces NO to N_2O in the process of reducing Pd, either directly or *via* an intermediate. The space-resolved average oxidation states of Pd according to LCA fits for gas conditions of 1000 ppm NO in argon and 1000 ppm NO and 10% O_2 in argon can be found in the ESI† (Fig. S3).

As XAS is a bulk sensitive technique, detailed mechanisms cannot be drawn solely from these data. In order to complement these measurements and provide a more complete insight into the mechanism under these dynamic conditions, the role of surface intermediates has been investigated in more detail by DRIFTS.

Operando DRIFTS measurements

Adsorption of NO. In order to identify the adsorbed NO species in the absence of any other reactive gases, DRIFTS measurements under a flow of NO and argon were performed (the uncorrected spectra are given in Fig. S4†). Several bands were found (summary given in Fig. 3), with high frequency species at 3777, 3733, 3691, and 3658 cm^{-1}, a broad water peak between 2500 and 3500 cm^{-1}, middle frequency bands at 2181, 2111, 2047, 1868, 1820, 1813, 1776, and 1745 cm^{-1}, and lower frequency bands at 1680, 1647, 1620, 1581, 1545, 1488, 1310, and 1270 cm^{-1}.

The negative bands between 3500 and 3800 cm^{-1} are assigned to OH-species, ν(OH),[54–56] with the 3733 and 3691 cm^{-1} bands associated with a loss of Ti^{4+}–OH and the 3658 cm^{-1} band with a loss of V–OH species. The bands associated with Ti–OH are more intense than those for V–OH. These bands become less intense at higher temperature, following the gradual disappearance of the broad water peak. The negative band at 2047 cm^{-1} is associated with 2ν(V═O) overtones and a loss of V^{5+} species within the catalyst.[56,57]

Bands at 2181 and 2111 cm^{-1} have generally been assigned to NO^+ on TiO_2 catalysts and linked to NO adsorption on Brønsted acid sites as a replacement of H^+ in OH species.[58,59] These bands are very weak relative to other bands (Fig. 4a) but are present in the greatest amount at temperatures where nitrates are more prevalent than Pd-adsorbed nitrosyls (Pd–NO), as described below. They are indicative of an oxidizing environment for NO. The band at 2181 cm^{-1} increases in intensity up to 175 °C before decreasing and disappearing by 250 °C, whereas the 2111 cm^{-1} band is most pronounced at 50 °C and vanishes above 175 °C. Both peaks redshift with increasing temperature, suggesting slight relaxation of the N–O bonds due to reduced constraints localized around the surface binding site.

The bands between 1725 and 1900 cm^{-1} are associated with linearly adsorbed NO on Pd and V, which have been previously reported at 1890 (V^{4+} $(NO)_2$, ν_s(NO)[60] and Pd^{2+} $(NO)_2$, ν_s(NO)[61]), 1828 (V^{3+} $(NO)_2$, ν_s(NO)),[56] 1830 (Pd^{2+}, ν(N═O)),[59] 1776 (V^{4+} $(NO)_2$, ν_{as}(NO)[62] and Pd^+, ν(NO)[55]), and 1745 cm^{-1} (V^{4+} $(NO)_2$, ν_{as}(NO)[56] and Pd^0, ν(NO)[55]). While there is potential overlap between Pd–NO and V–NO species, IR bands of nitrosyls are only seen on vanadium at or above ambient temperatures after substantial reduction of the catalyst.[56] A previous DRIFTS study by Macleod *et al.* on V_2O_5/Al_2O_3 with and without Pd concluded that V^{3+} and V^{4+}

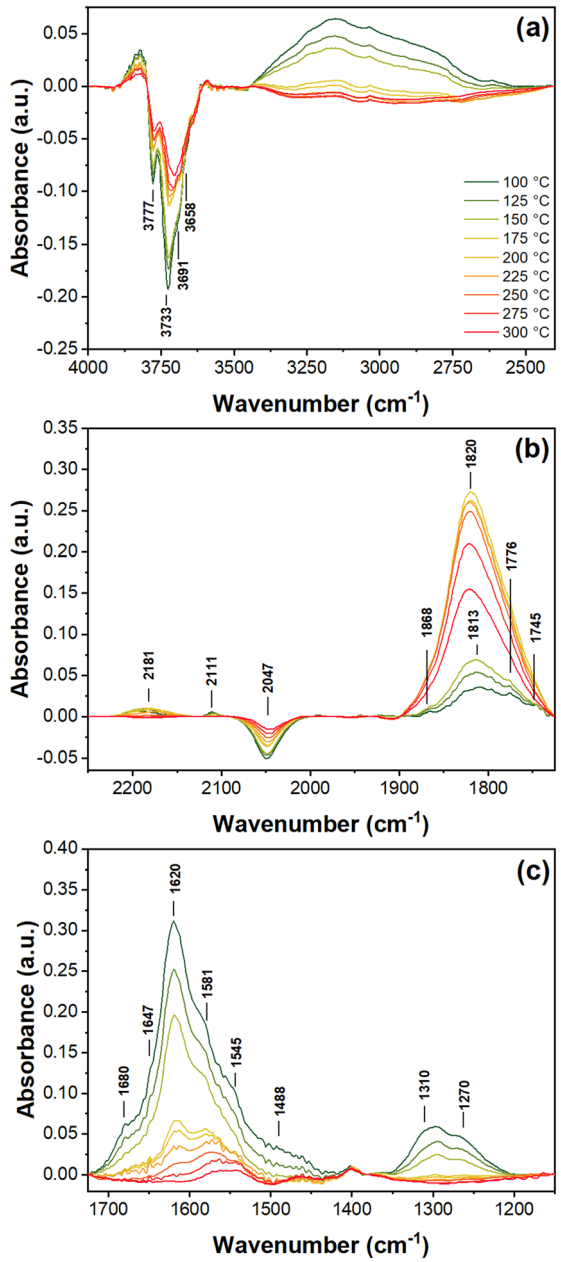

Fig. 3 Temperature dependent DRIFTS spectra of the 1%Pd/5%V_2O_5/20%TiO_2–Al_2O_3 catalyst under a flow of 1000 ppm NO in Ar, shown at (a) high wavenumbers for OH (negative) and water bands, (b) middle wavenumbers for NO^+, V=O (negative), and Pd–NO bands, and (c) low wavenumbers for support nitrate and nitrite bands.

centers do not form under H_2-SCR conditions (4000 ppm H_2, 500 ppm NO, 5% O_2), while also measuring a negative V^{5+} band at 2047 cm^{-1}.[33] Likewise, only nitrosyl bands for the Pd loaded catalyst were observed, and hence the bands at 1819 and 1788 cm^{-1} were assigned to Pd^+-NO. Considering these findings, it is reasonable to conclude that the bands between 1725 and 1900 cm^{-1} in the current study are predominantly due to NO species adsorbed on Pd.

In the case of the measurements reported herein, at low temperatures for the adsorption of NO on Pd, the peak at 1813 cm^{-1} (Pd^{n+}, Pd^{2+}(OH)NO, ν(NO))[63] is the predominant band. The blueshift of this peak to 1820 cm^{-1}, which occurred with increasing temperature, may be due to overlap among a combination of lesser bands at 1830 and 1828 cm^{-1} with the 1813 cm^{-1} band, suggesting a greater prevalence of Pd^{2+}. This corresponds to the slight oxidizing effect of NO on Pd when Pd is sufficiently reduced as seen by XAS (*cf.* Fig. S2e†). However, the dominance and symmetry of the 1820 cm^{-1} band above 150 °C makes it difficult to assign direct contribution of additional nitrosyl states under these conditions. At lower temperatures from 100 to 150 °C, weaker bands at 1745, 1776, and 1868 cm^{-1} may contribute asymmetry to the 1813 cm^{-1} band, as they are significant features observed under other gas conditions discussed in later sections below, but are not significant features during NO adsorption on this catalyst. At approximately 250 °C, the band intensity of Pd–NO moieties begins to decrease sharply. At these high temperatures, according to previous temperature programmed desorption (TPD) measurements of NO on Pd,[64] the rate of desorption of NO from Pd limits the presence of adsorbed nitrosyl species.

The negative band area at 2047 cm^{-1} decreases in unison with the shrinking of negative OH bands (3500–3800 cm^{-1}) and of low frequency bands from 1200 to 1650 cm^{-1}, which are assigned to different nitrate species ($\nu_3(NO_3)$). The bands at 1647 and 1620, 1581 and 1545, and 1310 and 1270 cm^{-1} correspond to bridging nitrates, bidentate nitrates, and monodentate nitrates, respectively.[55–58,65,66] Bands around 1680 cm^{-1} are not well established in the literature, but evolve in parallel with bridge nitrates, suggesting they are an additional bridging species (*e.g.* metal-support bridging nitrates). Additional smaller peaks near 1200 cm^{-1} may contribute to the broad band from 1350 to 1200 cm^{-1} due to ν_3 splitting of the bridge ($\Delta\nu_3 \sim 420$ cm^{-1}) and bidentate ($\Delta\nu_3 \sim 300$ cm^{-1}) species. The band at 1488 cm^{-1} has been previously seen in the literature, but doesn't have a clear assignment;[61,66] it can be a chelating nitrate or hydrogenated NO species such as NH_2NO, but unlikely to be ammonia species due to the lack of more intense bands at 1434 cm^{-1}.

On TiO_2 and V_2O_5 supports, it is generally understood that nitrates form *via* surface hydroxides and are the primary contributors towards the negative bands at 3500 to 3800 and 2047 cm^{-1},[57,58,65] following the reaction,

$$2Ti{-}OH + 2NO + 2[O] \rightarrow Ti{-}O{-}NO_2 + Ti{-}O{-}NO + H_2O \quad (1)$$

where [O] is surface oxygen, of which vanadium is a source. These previous reports are further substantiated by the band intensities of nitrates decreasing and approaching zero in concert with the those of OH and V^{5+}=O with increasing temperature (Fig. 4a). Among all the nitrate species, the bidentate nitrates at 1581 and 1545 cm^{-1} are the most stable and are still present in small amounts at 300 °C. The conditions under which nitrates are stable appear to be opposite for nitrosyl adsorption on Pd, as the bands between 1725 and 1900 cm^{-1} remained relatively weak until the nitrate bands

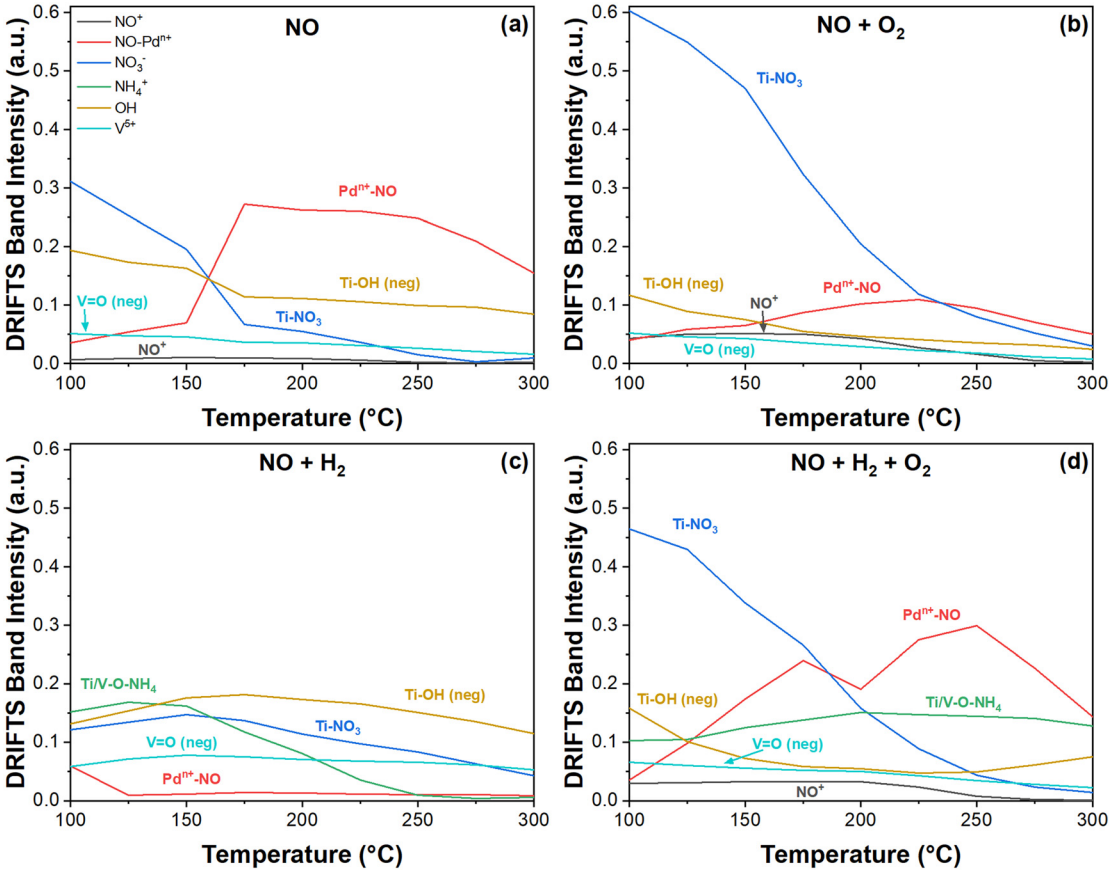

Fig. 4 Absolute intensities of selected IR bands of reactive intermediates from DRIFTS pseudo-absorbance spectra for (a) NO, (b) NO and O_2, (c) NO and H_2, and (d) SCR gas mixtures. The V^{5+} and OH bands are negative in absorbance and represent the relative decrease in V=O and Ti–OH species, respectively.

diminished at 175 °C. At the point when nitrate bands become less intense than Pd–NO nitrosyls, Pd begins to reduce NO_x species, supported by the disappearance of NO^+ bands and the gradual increase in Pd oxidation state as measured by XAS (*cf.* Fig. S3e†). Here it can be inferred that at lower temperatures, NO_x is more easily oxidized by the support and PdO, leading to more oxidized nitrogen species. As temperature increases, nitrates at the metal-support interface become reduced by Pd and form Pd^{n+}–NO nitrosyl species. These findings are observed to a greater extent with other gas conditions below.

Co-Adsorption of NO and O_2. Introduction of O_2 into the gas feed largely leaves the NO adsorption spectra unchanged (Fig. 5), with mostly changes in band intensity; the chemistry corresponding with OH bands, V^{5+} and NO^+ bands, and nitrate bands largely remain the same as with the NO condition. The addition of O_2 only leads to increased nitrate presence by oxidizing NO and makes the 1620 cm^{-1} bands more stable at higher temperatures as shown in Fig. 5b. The 1488 cm^{-1} band disappears and the 1310 cm^{-1} band redshifts to 1290 cm^{-1} as a lower frequency monodentate nitrate. Bidentate nitrates remain the most stable nitrate species and are the only nitrates remaining above 250 °C.

The most significant changes can be seen in the nitrosyl bands from 1725 to 1900 cm^{-1}, where the main similarity between the NO and NO + O_2 conditions is the desorption of NO from Pd above 250 °C. In the co-adsorption of NO and O_2, the splitting among bands at 1826 and 1813 cm^{-1} is more pronounced, and a new band emerges at 1796 cm^{-1}. These bands, as well as the 1776 cm^{-1} band, evolve in unison, increasing until 225 °C before gradually decaying with increasing temperature due to rapid desorption of NO from Pd. The maximum intensity of these bands is substantially less than with the adsorption of only NO. Also unlike in the previous gas condition, Pd gradually reduces with increasing temperature during the co-adsorption of NO and O_2, as shown by XAS (*cf.* Fig. S3b†), which correlates both with Pd–NO gradually increasing and a substantial presence of NO^+ from broad and intense bands at 2181 cm^{-1}. The oxidation state of Pd levels out and remains constant at 225 °C, at which point Pd–NO and NO^+ bands decrease.

From the combined observations of NO adsorption and NO and O_2 co-adsorption, it can be inferred that nitrosyl species on Pd form more easily from nitrates which are reduced by Pd, given the stronger Pd^{n+}–NO bands with NO alone. The slight reduction of PdO observed with the co-adsorption of NO and O_2 suggests that PdO is able to some degree oxidize and store NO_x. However, given the more significant oxidation of Pd and greater presence of nitrosyl

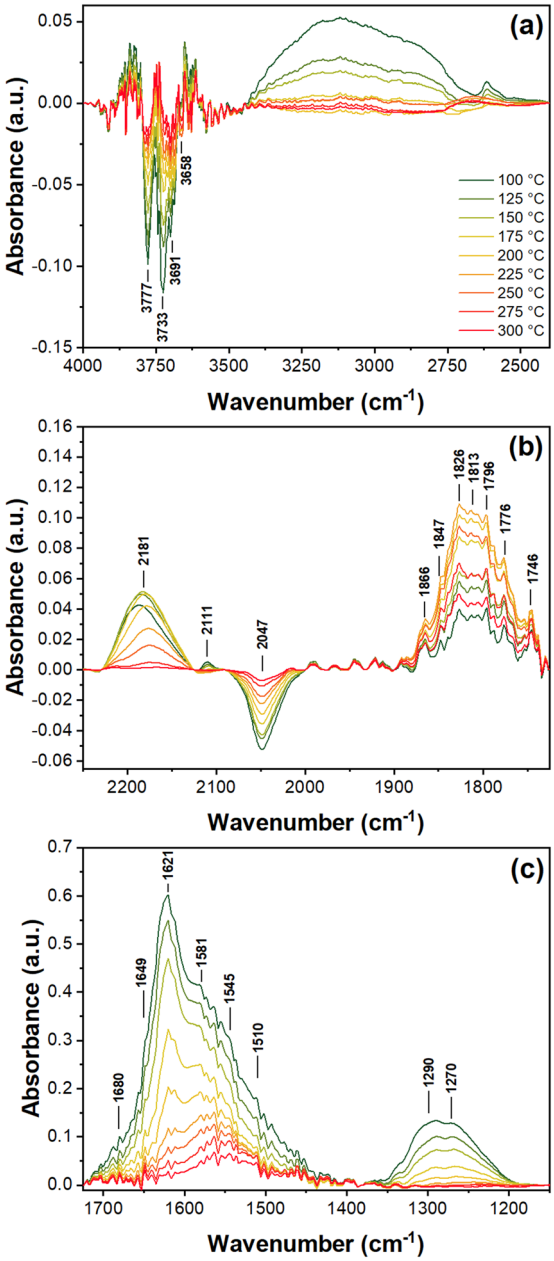

Fig. 5 Temperature dependent DRIFTS spectra of the 1%Pd/5%V_2O_5/20%TiO_2–Al_2O_3 catalyst under a flow of 1000 ppm NO and 10% O_2 in Ar, shown at (a) high wavenumbers for OH (negative) and water bands, (b) middle wavenumbers for NO^+, V=O (negative), and Pd–NO bands, and (c) low wavenumbers for support nitrate and nitrite bands.

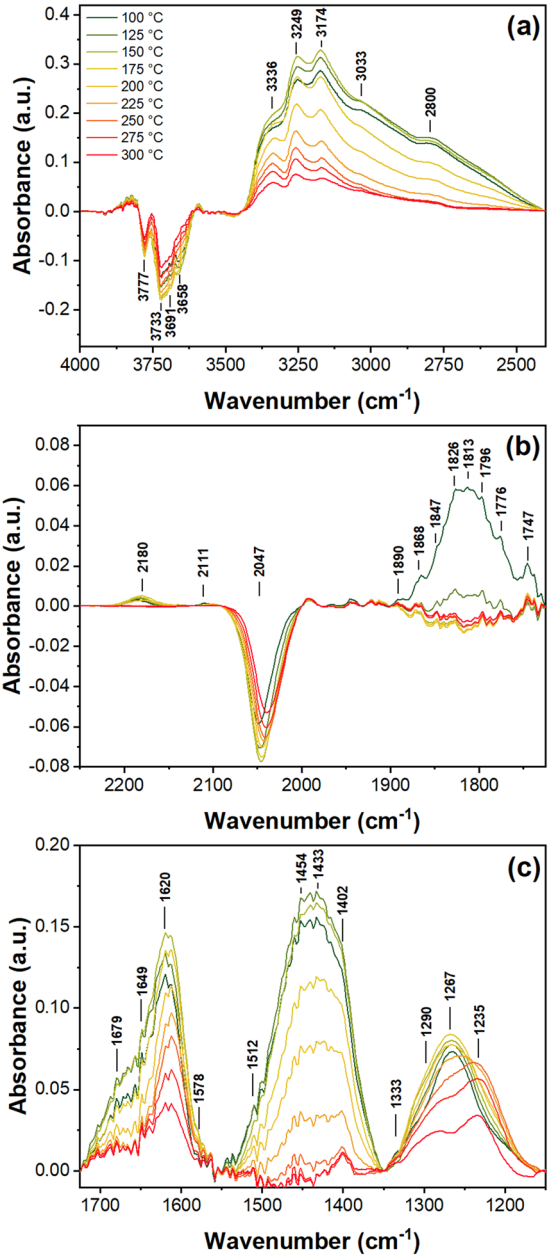

Fig. 6 Temperature dependent DRIFTS spectra of the 1% Pd/5%V_2O_5/20%TiO_2-Al_2O_3 catalyst under a flow of 1000 ppm NO and 5000 ppm H_2 in Ar, shown at (a) high wavenumbers for OH (negative), ammonia, and water bands, (b) middle wavenumbers for NO^+, V=O (negative), and Pd-NO bands, and (c) low wavenumbers for support nitrates, nitrites, and ammonia bands.

species on Pd, as observed during NO adsorption, it appears Pd more efficiently reduces surface NO_x.

Co-Adsorption of NO and H_2. The introduction of a strong reducing agent drastically changes the species observed in DRIFTS measurements. While most of the species described above are present to some degree, with exception to the bidentate nitrates which are almost fully absent except for a weak band at 1578 cm^{-1}, several new peaks appear at 3336, 3249, 3174, 3033, and 2800 cm^{-1} (Fig. 6a), 1890 cm^{-1} (Fig. 6b), and 1512, 1454, 1433, 1402, 1333, and 1235 cm^{-1} (Fig. 6c).

The bridging nitrate species are present at all measured temperatures, and the bands decrease slightly with increasing temperature, matching well with the negative OH and V^{5+} bands. Despite the apparent stability of nitrate species under reducing conditions, the overall intensities of these bands are substantially less than during the co-adsorption of NO and O_2. Additionally, the lower wavenumber bidentate nitrate species are largely absent at all temperatures, indicating their relative instability under

reducing conditions. Signs of altered nitrate chemistry are given by the blueshift of the OH bands and redshift of the V^{5+} bands with increasing temperature. An additional sign of altered chemistry is the presence of a monodentate nitrite band $\nu_3(NO_2)$ at 1512 cm^{-1}, which is relatively weak and rapidly vanishes with increasing temperature.

Unlike the previously discussed gas conditions, the Pd^{n+}–NO band at 1813 cm^{-1} was observed at 100 °C and rapidly vanished by 150 °C, along with neighboring and less intense Pd^{2+}, Pd^{+}, and Pd^{0} bands at 1868, 1776, and 1747 cm^{-1}, respectively, (Fig. 6b). The pathway through which NO adsorbs onto Pd under these reducing conditions at these temperatures is not clear, as both the average oxidation state of Pd (Fig. 1c) and nitrosyl bands (Fig. 4c) decrease simultaneously, but the overall lack of NO^{+} and low presence of nitrates suggests that NO is more likely reduced while adsorbing onto Pd. Additionally, the presence of H_2 without O_2 causes these linearly adsorbed species to be highly unstable and are likely converted into ammonia species, explained in more detail below.

New peaks from 2500 to 3500 cm^{-1} and 1350 to 1500 cm^{-1} are all associated with the formation of ammonium ions (NH_4^{+}) on Brønsted acid sites and NH_3 adsorbed on Lewis acid sites. It is well reported in the literature that the 3358 and 3240 cm^{-1} bands belong to the ν_s(N–H) modes, of NH_3 on Lewis sites, whereas the 3183, 3033, and 2800 cm^{-1} bands are for the ν_{as}(N–H), ν_{as}(N–H), and $2\delta_{as}$(H–N–H) modes, respectively, of NH_4^{+} adsorbed on Brønsted acid sites.[57,60,66,67] Lower frequency NH_4^{+} δ_{as}(H–N–H) modes are found at 1454, 1433, and 1402 cm^{-1},[67] with a corresponding δ_s(H–N–H) mode at 1660 cm^{-1}.[33] Low frequency modes of NH_3 adsorbed on Lewis acid sites, which overlap with the bands of monodentate nitrates at 1297, 1282, and 1256 cm^{-1}, are particularly difficult to isolate but may contribute to band broadening near 1300 cm^{-1}. A weak band at 1333 cm^{-1} is observed with questionable significance and may be attributed to nitro-compounds or N–N vibrations of *cis*-N_2O_2 species.[58] In the case of nitro-compounds, an additional band at 1580 cm^{-1} would be expected, but overlaps significantly with nitrate species. N_2O_2 species would have counterpart bands below 1050 cm^{-1} which is below the sample cut-off. During the co-adsorption of NO and H_2, this band is of questionable value but becomes more significant under SCR conditions, as discussed in detail below, suggesting it belongs to features of partially reduced NO_x species which are not observed in the absence of H_2.

NH_4^{+} adsorbed on Brønsted acid sites remain stable until around 200 °C, where they decay following the rapid reduction of Pd, as shown in Fig. 1c and 4c. By 250 °C, Pd is fully reduced and negligible NH_4^{+} remains on Brønsted acid sites. Beyond 250 °C and when NO approaches full conversion, only the bands at 1402, 3174, 3249, and 3336 cm^{-1} remain. The more intense modes of NH_3 adsorbed on Lewis acid sites suggest these as the dominant surface ammonia species. The decay curve of NH_4^{+} species matches that of N_2O in Fig. 1a, suggesting that NH_4^{+} is a critical intermediate for the formation of N_2O. The dependence of ammonium ions on oxidized Pd suggest NH_4^{+} forms at the metal-support interface *via* the reduction of NO_x species bridging PdO and TiO_2 Brønsted acid sites with activated hydrogen. These interfacial NH_4^{+} are then able to react with nitrates bridging PdO and TiO_2, forming N_2O *via* the following mechanism:[68]

$$NH_4^{+} + NO_3^{-} \rightarrow N_2O + 2H_2O \quad (2)$$

Once bulk reduced Pd appears (*cf.* Fig. 1c), ammonium ions are unable to form – as indicated by the disappearance of NH_4^{+} (1433 cm^{-1}) bands (*cf.* Fig. 4c and 6c) – and activated hydrogen becomes the dominant reducing agent, fully reducing nitrosyls and nitrates to N_2 and H_2O and eliminating N_2O as a product. Also under these conditions, trace amounts of N_2O in the gas phase are easily converted.

NH_3 adsorbed on Lewis acid sites becomes the dominant ammonia species at high temperatures, as indicated by lingering bands at 3249 and 3336 cm^{-1}. This suggests that Lewis acid sites on the support are not significantly impacted by the state of Pd and that NH_3 is a more stable reactive intermediate than NH_4^{+} at high temperatures. No significant gaseous NH_3 was detected in the MS data (m/z = 15), which could indicate that NH_3 adsorbed at Lewis acid sites on the titania–vanadia support performs SCR of NO_x in parallel with activated H_2 on Pd, matching previous reports;[28] however, this cannot be confidently concluded due to limitations in measuring small quantities of nitrogen species, especially in the case of NH_3, which has only a minor fragmentation ion at m/z = 15.

***In situ* DRIFTS of the H_2-SCR of NO.** With the addition of oxygen to the NO/H_2 mixture, which results in typical SCR conditions, no new bands appeared in DRIFTS spectra (Fig. 7). However, the temperature evolution of active metal–NO, ammonia, and nitrate modes are distinct, and aspects of each condition are visible and help elucidate the complex chemistry observed. The temperature dependence of bridge nitrates (1620 cm^{-1}), Pd–NO (1813 cm^{-1}), NO^{+} (2182 cm^{-1}), OH^{-} (3733 cm^{-1}), V^{5+} (2047 cm^{-1}), NH_4^{+} (1427 cm^{-1}), and NH_3 (1385 cm^{-1}) IR modes are shown in Fig. 4d and contrast with the other gas conditions in Fig. 4a–c.

Similar to the observations of the previously discussed gas mixtures (*cf.* Fig. 4), the negative OH and V^{5+} bands decrease in absolute area alongside the bridge nitrate bands with increasing temperature. However, the competition between NH_4^{+} and nitrates for adsorbing on Brønsted acid sites is more pronounced; from 50 to 100 °C, where NH_4^{+} species (1427 cm^{-1}) are most prevalent, the bridge and bidentate nitrate bands are less intense and grow in intensity from 125 °C as adsorbed NH_4^{+} decreases in prevalence. Additionally, the 1620 cm^{-1} bridge species undergoes a slight blueshift in the presence of NH_4^{+} at 50 and 75 °C. The clash between these molecules further suggests that bridge and bidentate nitrates form at Brønsted acid sites and compete with NH_4^{+}. In the absence of O_2, NH_4^{+} species dominate at low temperatures.

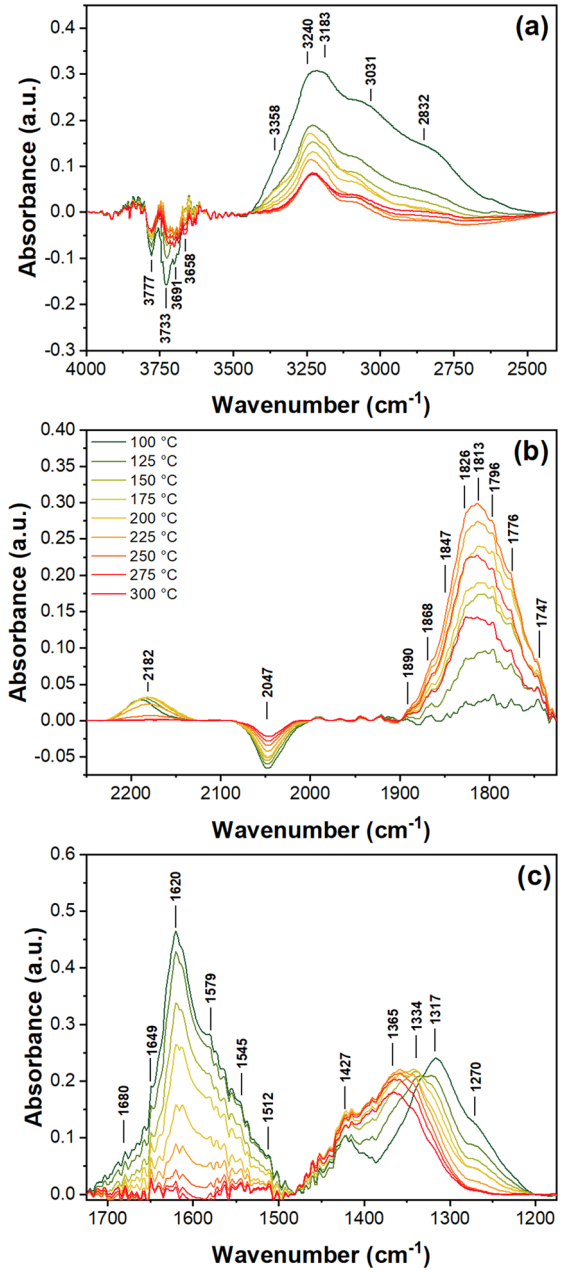

Fig. 7 Temperature dependent DRIFTS spectra of the 1%Pd/5%V_2O_5/20%TiO_2–Al_2O_3 catalyst under a flow of 1000 ppm NO, 5000 ppm H_2, and 10% O_2 in Ar, shown at (a) high wavenumbers for OH (negative), ammonia, and water bands, (b) middle wavenumbers for NO^+, V=O (negative), and Pd–NO bands, and (c) low wavenumbers for support nitrates, nitrites, and ammonia bands.

The presence of O_2 does not appear to lower the stability of NH_4^+ species, considering that the band intensities at 1427 and 3031 cm^{-1} are equal or higher than observed with just the NO + H_2 condition. O_2 rather promotes the formation of nitrates and causes the low frequency bands of NH_4^+ adsorbed on Brønsted acid sites to redshift with increasing temperature. It is important to note that the presence of O_2 also promotes NH_4^+ species at higher temperatures. Under the NO + H_2 condition, NH_4^+ species nearly fully diminished by 275 °C, whereas the low frequency NH_4^+ band at 1427 cm^{-1} remains present in significant amounts at 300 °C with the addition of O_2. No significant change was observed in the MS intensity of N_2O which suggests O_2 limits the conversion of NH_x species to N_2O. However, the small amounts of N_2O expected from this catalyst (*i.e.* 50 ppm)[34] during SCR of NO_x was not detected by MS.

Another significant change due to the addition of O_2 to the NO + H_2 mixture is the more significant presence of bands between 1300 and 1400 cm^{-1}, which undergo a blueshift with increasing temperatures. The band at 1317 cm^{-1}, generally assigned to monodentate nitrates on TiO_2, is significant at 50 °C but gradually decreases and seemingly shifts to 1334 cm^{-1} at 175 °C and ultimately 1365 cm^{-1} by 300 °C. Part of this shift can be explained by diminishing nitrate bands throughout the entire spectrum. However, the blueshift to frequencies closer to 1365 cm^{-1} correlates with the onset of SCR activity at 200 °C (Fig. 1b), and all bands around 1365 cm^{-1} begin to decrease in intensity as NO conversion decreases beyond 250 °C. Here it can be inferred that more complex partially reduced N_xO_y species (*e.g.* nitro-compounds,)[55,58] are formed as SCR intermediates.

The bands for active metals from 1725 and 1900 cm^{-1} indicate/support three temperature regimes relevant for the performance of the H_2-SCR reaction. Similar to the NO and NO + O_2 conditions, the Pd–NO bands are largely absent until the bridge nitrate species at 1649 and 1620 cm^{-1} significantly decrease. In this low temperature regime, below 200 °C and the onset of SCR activity, the abundance of nitrates and NO^+ species suggests that NO is more favorably oxidized. Given the gradual reduction of Pd, as shown by XANES in Fig. 1d and as observed during the co-adsorption of NO and O_2, PdO appears able to oxidize NO_x and form metal-support bridge nitrates (1680 cm^{-1}) according to eqn (1). This then is an intermediate step towards the formation of Pd–NO nitrosyls. After the onset of SCR activity above 200 °C, nitrates and NO^+ species diminish, converting to nitrosyl species on Pd and forming PdO, as observed in the adsorption of NO alone. Above 250 °C, SCR activity decreases in intensity, Pd–NO IR bands rapidly shrink, and the average oxidation state of Pd begins to significantly decline. Here, as observed with the adsorption of NO and the co-adsorption of NO and O_2, the rate of desorption of NO limits the presence of NO species on the active metal. In turn, activated hydrogen on bulk reduced Pd more readily reduces Pd and combusts with impinging O_2.

It is notable that the conversion of NO decreases less drastically as the desorption of NO from Pd and the reduction of Pd. This can be explained by the role of the titania–vanadia support, which has been previously shown to reduce NO_x at high temperatures without the presence of active metal.[26] To this end, NH_3 adsorbed on Lewis acid sites, indicated by the persistent band at 3240 cm^{-1}, is a species which exists independently of the state of Pd which is efficient at reducing NO_x stored on the TiO_2 support during H_2-SCR.[28]

These findings point towards Pd^{n+}–NO as the active surface intermediate for H_2-SCR activity on the active

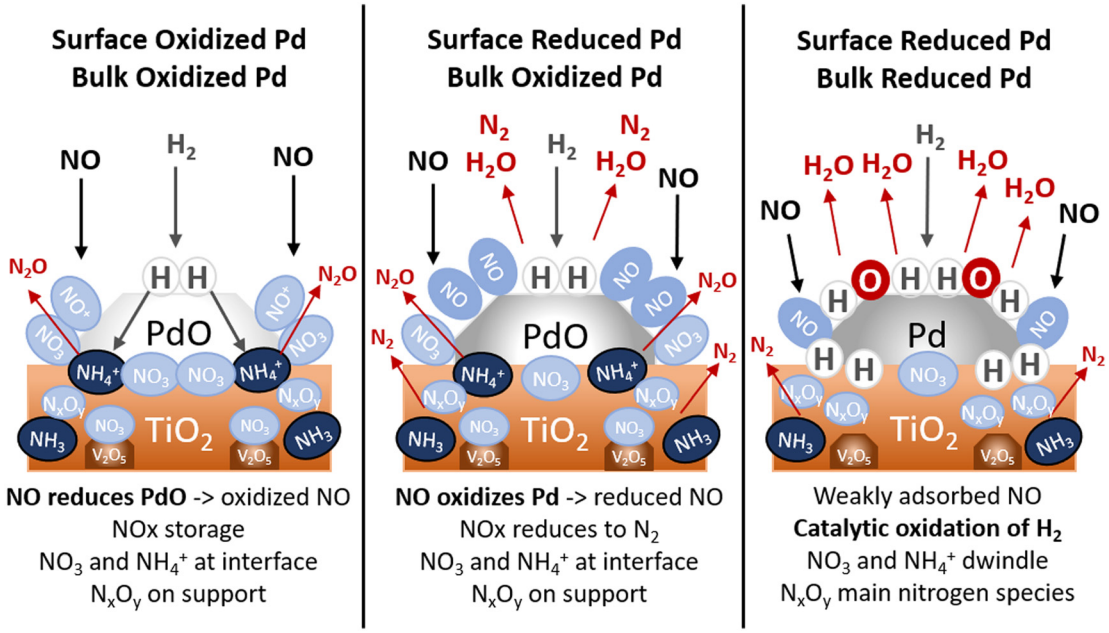

Scheme 1 Evolution of nitrogen species on $Pd/V_2O_5/TiO_2$–Al_2O_3 with respect to Pd oxidation state.

metal and NH_3 adsorbed onto Lewis acid sites as an active intermediate for SCR on the support. Notably, at 250 °C where NO conversion is maximized, the nitrosyl (1796, 1813, and 1826 cm^{-1}) bands are also at their maximum intensity. When the temperature increases, NO conversion weakens and Pd becomes more reduced due to runaway activation of H_2 and its subsequent catalytic oxidation, which correlates with the decrease in the area of all three IR bands. Despite the rapid reduction of Pd, the presence of O_2 slows this reduction relative to what was observed during the co-adsorption of NO and H_2. This suggests that O_2 buffers the Pd state during SCR, delaying and limiting the rate of reduction.

Conclusions

The average oxidation state of Pd on a 1%Pd/5%V_2O_5/20%TiO_2-Al_2O_3 catalyst create three distinct regimes and plays a pivotal role in which adsorbed species exist on the surface and which reaction pathways for NO_x reduction occur during H_2-SCR (*cf.* Scheme 1). The prevalence of PdO on the surface and in the bulk material, mediated by the presence of O_2, influence how NO_x is stored and reacts with adsorbed reducing agents.

In the case of mostly oxidized Pd, where both the surface and bulk are PdO-like, gradual reduction of Pd was observed during adsorption of NO, both with and without O_2. This coincided with the formation of NO^+ ions and nitrates, demonstrating that NO is able to reduce PdO. While Pd^{n+}–NO adsorbates were observed under these conditions, oxidation of NO favors the formation of other nitrogen species (*e.g.* nitrates, nitrites, nitro-compounds) which store at the metal-support interface or on the metal oxide. Highly oxidized Pd is not directly conducive to SCR, either due to stable NO_x adsorbates in the presence of O_2 or due to the formation of undesired N_2O from the combination of NH_4^+ and nitrates at the metal-support interfacial Brønsted acid sites.

The SCR of NO is most efficient on slightly reduced Pd, in which the surface contains a significant amount of Pd^0 for NO_x adsorbates to oxidize. Metal-support bridged nitrates react with Pd^0 to form adsorbed Pd^{n+}–NO. H_2 then further reduces these nitrosyl species to H_2O and N_2. Partially reduced adsorbed N_xO_y species (*e.g.* nitro-compounds) are also present in significant amounts under SCR conditions when Pd is also partially reduced.

Once bulk PdO is reduced to metallic Pd, both O_2 and H_2 activate and catalytic oxidation of H_2 becomes the favored reaction pathway. At temperatures above 250 °C, the fast desorption of NO from Pd outpaces the ability for nitrates to oxidize Pd, further inhibiting SCR activity and causing a runaway reduction of Pd.

Ammonium ions adsorbed on Brønsted acid sites at the Pd-support interface, are highly affected by the Pd oxidation state. In the absence of O_2, NH_4^+ ions are not formed on reduced Pd. The presence of O_2 stabilizes adsorbed ammonium and restricts the undesired conversion to N_2O.

NH_3 adsorbed on Lewis acid sites exists independent of the Pd state, with or without O_2.

Here the vanadia–titania support plays a critical role in the SCR of NO by oxidizing impinging NO and storing it on the surface as stable nitrates and nitrites at Brønsted acid sites. V=O readily oxidizes NO across all measured temperatures both in the presence and absence of O_2. The Lewis acid sites on TiO_2 also permit stable NH_3 formation in the presence of H_2, which selectively reduce absorbed NO_x to N_2 at high temperatures when NO desorbs from the active metal.

From the data presented herein, in order to optimize SCR of NO_x by H_2, metal-support bridge nitrates need to be the focus as they are a form of NO_x storage as well as a critical intermediate for nitrosyls on the active metal. This would require increased Brønsted acid site prevalence near or at the active metal interface. However, it should be kept in mind that these sites are susceptible to NH_4^+ ions and N_2O formation especially under rich exhaust conditions. With sufficient O_2, the sites will ultimately increase the amount of desired reactive intermediates and therefore increase catalytic activity.

Data availability

Processed data supporting conclusions is available in the manuscript and the ESI.† Raw data can be provided by the authors upon a reasonable request.

Author contributions

Thomas Eldridge: writing – original draft, visualization, validation, data curation, methodology, investigation. Michael Borchers: methodology, investigation. Patrick Lott: writing – review & editing. Jan-Dierk Grunwaldt: writing – review & editing, funding acquisition, resources, supervision. Dmitry Doronkin: writing – review & editing, validation, methodology, investigation, supervision.

Conflicts of interest

There are no conflicts to declare.

Acknowledgements

The work has been supported by the Helmholtz Association through the MTET (Materials and Technologies for Energy Transition) program. We acknowledge DESY (Hamburg, Germany), a member of the Helmholtz Association HGF, for the provision of experimental facilities. Parts of this research were carried out at PETRA III and we would like to thank Dr. Aleksandr Kalinko and Dr. Wolfgang Caliebe for assistance in using beamline P64. Beamtime was allocated for proposal I-20220246. We thank Dr. Olaf Deutschmann for provision of infrastructure, resources, and fruitful discussion.

References

1 G. Ertl, H. Knözinger and J. Weitkamp, *Handbook of heterogeneous catalysis*, VCH Weinheim, 1997.
2 K. F. Kalz, R. Kraehnert, M. Dvoyashkin, R. Dittmeyer, R. Gläser, U. Krewer, K. Reuter and J.-D. Grunwaldt, *ChemCatChem*, 2017, **9**, 17–29.
3 C. M. White, R. R. Steeper and A. E. Lutz, *Int. J. Hydrogen Energy*, 2006, **31**, 1292–1305.
4 S. Verhelst, P. Maesschalck, N. Rombaut and R. Sierens, *Int. J. Hydrogen Energy*, 2009, **34**, 4406–4412.
5 R. Jeeragal and K. A. Subramanian, *J. Therm. Sci.*, 2019, **28**, 789–800.
6 K. W. Scholl and S. C. Sorenson, *SAE Trans.*, 1993, 1450–1462.
7 I. Nova, C. Ciardelli, E. Tronconi, D. Chatterjee and B. Bandl-Konrad, *Catal. Today*, 2006, **114**, 3–12.
8 A. Grossale, I. Nova, E. Tronconi, D. Chatterjee and M. Weibel, *J. Catal.*, 2008, **256**, 312–322.
9 M. Colombo, I. Nova and E. Tronconi, *Catal. Today*, 2012, **197**, 243–255.
10 T. Günter, H. W. Carvalho, D. E. Doronkin, T. Sheppard, P. Glatzel, A. J. Atkins, J. Rudolph, C. R. Jacob, M. Casapu and J.-D. Grunwaldt, *Chem. Commun.*, 2015, **51**, 9227–9230.
11 O. Deutschmann and J.-D. Grunwaldt, *Chem. Ing. Tech.*, 2013, **85**, 595–617.
12 A. Boubnov, H. W. P. Carvalho, D. E. Doronkin, T. Günter, E. Gallo, A. J. Atkins, C. R. Jacob and J.-D. Grunwaldt, *J. Am. Chem. Soc.*, 2014, **136**, 13006–13015.
13 Y. Ganjkhanlou, T. V. W. Janssens, P. N. R. Vennestrøm, L. Mino, M. C. Paganini, M. Signorile, S. Bordiga and G. Berlier, *Appl. Catal., B*, 2020, **278**, 119337.
14 Z. Liu, J. Wu and C. Hardacre, *Catal. Surv. Asia*, 2018, **22**, 146–155.
15 Z. Hu and R. T. Yang, *Ind. Eng. Chem. Res.*, 2019, **58**, 10140–10153.
16 J.-D. Grunwaldt, N. V. Vegten and A. Baiker, *Chem. Commun.*, 2007, 4635–4637.
17 E. K. Dann, E. K. Gibson, R. H. Blackmore, C. R. A. Catlow, P. Collier, A. Chutia, T. E. Erden, C. Hardacre, A. Kroner, M. Nachtegaal, A. Raj, S. M. Rogers, S. F. R. Taylor, P. Thompson, G. F. Tierney, C. D. Zeinalipour-Yazdi, A. Goguet and P. P. Wells, *Nat. Catal.*, 2019, **2**, 157–163.
18 C. N. Costa and A. M. Efstathiou, *Environ. Chem. Lett.*, 2004, **2**, 55–58.
19 C. N. Costa and A. M. Efstathiou, *J. Phys. Chem. B*, 2004, **108**, 2620–2630.
20 C. N. Costa and A. M. Efstathiou, *Appl. Catal., B*, 2007, **72**, 240–252.
21 G. G. Olympiou and A. M. Efstathiou, *Chem. Eng. J.*, 2011, **170**, 424–432.
22 P. Wu, L. Li, Q. Yu, G. Wu and N. Guan, *Catal. Today*, 2010, **158**, 228–234.
23 D. T. Koch, E. Eßer, S. Kureti and A. Sousa, *Motortech. Z.*, 2020, **81**, 32–39.
24 B. Wen, *Fuel*, 2002, **81**, 1841–1846.
25 G. Qi, R. T. Yang and L. T. Thompson, *Appl. Catal., A*, 2004, **259**, 261–267.
26 G. Qi, R. T. Yang and F. C. Rinaldi, *J. Catal.*, 2006, **237**, 381–392.
27 L. Wang, C. Yin and R. T. Yang, *Appl. Catal., A*, 2016, **514**, 35–42.
28 Z. Hu, X. Yong, D. Li and R. T. Yang, *J. Catal.*, 2020, **381**, 204–214.
29 V. K. Patel and S. Sharma, *Catal. Today*, 2021, **375**, 591–600.
30 A. Ueda, T. Nakao, M. Azuma and T. Kobayashi, *Catal. Today*, 1998, **45**, 135–138.
31 R. Burch and M. D. Coleman, *Appl. Catal., B*, 1999, **23**, 115–121.

32 K. Duan, Z. Wang, C. Hardacre, Z. Liu, S. Chansai and C. Stere, *Catal. Today*, 2019, **332**, 69–75.
33 N. Macleod and R. M. Lambert, *Catal. Lett.*, 2003, **90**, 111–115.
34 M. Borchers, K. Keller, P. Lott and O. Deutschmann, *Ind. Eng. Chem. Res.*, 2021, **60**, 6613–6626.
35 F. J. P. Schott, P. Balle, J. Adler and S. Kureti, *Appl. Catal., B*, 2009, **87**, 18–29.
36 M. Leicht, F. J. P. Schott, M. Bruns and S. Kureti, *Appl. Catal., B*, 2012, **117–118**, 275–282.
37 C. Hahn, M. Endisch, F. J. P. Schott and S. Kureti, *Appl. Catal., B*, 2015, **168–169**, 429–440.
38 C. Hahn, M. Endisch and S. Kureti, *Top. Catal.*, 2017, **60**, 238–242.
39 T. Nanba, C. Kohno, S. Masukawa, J. Uchisawa, N. Nakayama and A. Obuchi, *Appl. Catal., B*, 2003, **46**, 353–364.
40 H. Hamada and M. Haneda, *Appl. Catal., A*, 2012, **421–422**, 1–13.
41 Z. Hong, X. Sun, Z. Wang, G. Zhao, X. Li and Z. Zhu, *Catal. Sci. Technol.*, 2019, **9**, 3994–4001.
42 M. Borchers, P. Lott and O. Deutschmann, *Top. Catal.*, 2023, **66**, 973–984.
43 L. Zhang, Y. Shan, Z. Yan, Z. Liu, Y. Yu and H. He, *J. Environ. Sci.*, 2024, **138**, 102–111.
44 H. Topsøe, *J. Catal.*, 2003, **216**, 155–164.
45 A. Urakawa, N. Maeda and A. Baiker, *Angew. Chem., Int. Ed.*, 2008, **47**, 9256–9259.
46 L. van Beek, D. Jain, P. Gholkar, T. J. Eldridge, H. P. Nguyen, K. Muramoto and A. Urakawa, *Catal. Today*, 2024, **429**, 114466.
47 A. M. Gänzler, M. Casapu, D. E. Doronkin, F. Maurer, P. Lott, P. Glatzel, M. Votsmeier, O. Deutschmann and J.-D. Grunwaldt, *J. Phys. Chem. Lett.*, 2019, **10**, 7698–7705.
48 B. Bornmann, J. Kläs, O. Müller, D. Lützenkirchen-Hecht and R. Frahm, *AIP Conf. Proc.*, 2019, **2054**, 040008.
49 D. E. Doronkin, H. Lichtenberg and J.-D. Grunwaldt, *XAFS Techniques for Catalysts, Nanomaterials, and Surfaces*, 2017, pp. 75–89.
50 D. Lützenkirchen-Hecht, J.-D. Grunwaldt, M. Richwin, B. Griesebock, A. Baiker and R. Frahm, *Phys. Scr.*, 2005, **2005**, 831.
51 M. Newville, Larch: an analysis package for XAFS and related spectroscopies, *J. Phys.: Conf. Ser.*, 2013, **430**, 012007.
52 B. Ravel and M. Newville, *J. Synchrotron Radiat.*, 2005, **12**, 537–541.
53 A. Puig-Molina, F. M. Cano and T. V. W. Janssens, *J. Phys. Chem. C*, 2010, **114**, 15410–15416.
54 M. Kantcheva, *J. Catal.*, 2001, **204**, 479–494.
55 J. M. Watson and U. S. Ozkan, *J. Catal.*, 2002, **210**, 295–312.
56 K. Hadjiivanov, P. Concepción and H. Knözinger, *Top. Catal.*, 2000, **11**, 123–130.
57 L. Chen, J. Li and M. Ge, *J. Phys. Chem. C*, 2009, **113**, 21177–21184.
58 K. Hadjiivanov and H. Knözinger, *Phys. Chem. Chem. Phys.*, 2000, **2**, 2803–2806.
59 R. F. Ilmasani, J. Woo, D. Creaser and L. Olsson, *Ind. Eng. Chem. Res.*, 2020, **59**, 9830–9840.
60 M. A. Centeno, I. Carrizosa and J. A. Odriozola, *Appl. Catal., B*, 2001, **29**, 307–314.
61 Y. Zhang, S. Xu, J. Li, E. He and Z. Liu, *J. Phys. Chem. C*, 2023, **127**, 7248–7256.
62 M. A. Matsko, I. P. Prosvirin, T. B. Mikenas, V. A. Zakharov, E. A. Paukshits, V. I. Bukhtiyarov and I. G. Danilova, *J. Mol. Catal. A: Chem.*, 2000, **158**, 443–446.
63 I. Song, K. Khivantsev, Y. Wang and J. Szanyi, *J. Phys. Chem. C*, 2022, **126**, 1439–1449.
64 H. D. Schmick and H. W. Wassmuth, *Surf. Sci.*, 1982, **123**, 471–490.
65 K. Hadjiivanov, V. Bushev, M. Kantcheva and D. Klissurski, *Langmuir*, 1994, **10**, 464–471.
66 N. Macleod, R. Cropley and R. M. Lambert, *Catal. Lett.*, 2003, **86**, 69–75.
67 C.-H. Lin and H. Bai, *Appl. Catal., B*, 2003, **42**, 279–287.
68 J. Luo, Y. Tang, S. Joshi, K. Kamasamudram, N. Currier and A. Yezerets, *SAE Int. J. Engines*, 2017, **10**, 1691–1696.

